Hindawi
Journal of Nanomaterials
Volume 2023, Article ID 9266072, 14 pages
https://doi.org/10.1155/2023/9266072

Research Article

Investigation of Different Configurations in GeSe Solar Cells for Their Performance Improvement

A. Bala Sairam,[1,2] **Yogesh Singh**,[2,3] **Mamta**,[2,3] **Manoj Kumar**,[2,3] **Sanju Rani**,[2,3] **and V. N. Singh**[2,3]

[1]*Amity University Haryana, Gurugram 122413, India*
[2]*Indian Reference Materials (BND) Division, National Physical Laboratory, Council of Scientific and Industrial Research (CSIR), Dr. K.S. Krishnan Road, New Delhi 110012, India*
[3]*Academy of Scientific and Innovative Research (AcSIR), National Physical Laboratory, Dr. K.S. Krishnan Road, New Delhi 110012, India*

Correspondence should be addressed to V. N. Singh; singhvn@nplindia.org

Received 19 August 2022; Revised 3 November 2022; Accepted 10 November 2022; Published 4 January 2023

Academic Editor: Van Viet Pham

Thin-film-based photovoltaics offer affordable solar panels (high energy output per unit cost). Various materials have been used for thin-film solar cells, and still, new materials are being tested. In this work, the overall performance of GeSe is enhanced theoretically from a generic solar structure to a configuration that yields a whopping 33.12% efficiency along with an open circuit voltage of 1.04 V by optimizing various active layers using solar cell capacitance simulator SCAPS. The results have been explained most simply, utilizing the physics behind introducing hole transport layers in solar cells. The work also shows how certain contradictions in parameter values in the literature of GeSe can influence the cell's performance. The result shows why the substrate structure is better than the superstrate structure. Most of the reported results are on superstrate structure, which might have caused poor performance in previously experimentally produced GeSe solar cells.

1. Introduction

The boom of twenty-first-century technology is becoming the doom of the other centuries to ever come in the future due to global warming and the energy crisis. It puts us in a position to invest in low-cost and high-benefit renewable energy sources. It is the point where thin-film photovoltaics (TFPVs) steps in. Ideally, silicon-based solar cells can attain an efficiency of 34%, but the PV community has been able to design a cell with 24.7% efficiency till now [1]. This value is even lower for polycrystalline Si PVs. We already know that commercial solar PV panels' efficiency deteriorates with time [2]. Silicon PVs are comparably costly to TFPVs because of the absorption coefficient of silicon. The bandgap of silicon is 1.13 eV [3]. It means that silicon can use the photons having energy equal to and more than 1.13 eV for electron–hole pair generation. The corresponding wavelength of these photons with energy equal to and more than 1.13 eV falls from about 1,090 nm to 400 nm, which covers almost the entire solar spectrum. Its absorption coefficient, which is a function of wavelength, is as high as 10^5 at 400 nm (high energy photons) but decreases radically to 10^1 at 1,000 nm (low energy photons) [4, 5]. Since the absorption depth is the inverse of the absorption coefficient, the low-wavelength photons get absorbed near the surface while the high-wavelength photons get absorbed deeper from the surface. So, to absorb the entire solar spectrum, researchers are forced to design a solar cell with a thicker silicon layer to generate the maximum electron–hole pairs possible. It is the parameter that makes conventional silicon solar cells thicker (~2,00,000 μm), leading to more material for production, which in turn leads to more manufacturing costs [2, 3, 6]. The high thickness is also why integrated silicon-based devices are hard to manufacture [6]. However, when it comes to the absorber materials used in TFPV cells (including modified or doped silicon), their absorption coefficient ranges from 10^5 to 10^3 for the intended wavelength range [7]. So, the layer can be thin (~2 μm) and still be able to absorb as well as silicon. Thus, TFPV has more energy output per unit cost [8]. Cadmium tellurium (CdTe) and

copper indium gallium selenide are other majorly used absorbers for PV cells. They have high efficiency of about 22% [9, 10]. Both are inferior to GeSe because indium and gallium are rare earth metals, and cadmium is highly toxic. Antimony triselenide (Sb_2Se_3) and germanium monoselenide/germanium selenide (GeSe) are some of the best absorbers suitable for TFPV applications. Both have an orthorhombic structure, but Sb_2Se_3 is a V–VI type compound, making its structure more complex than GeSe. The Earth's abundance of Ge is six times that of Sb, resulting in a lower raw cost of Ge than Sb [11]. The high chemical stability of GeSe arises due to its crystallization process, which happens to be layered [12]. This less-toxic chalcogenide belongs to the IV–VI compound with a high absorption coefficient at room temperature [13, 14]. Low-cost preparation of GeSe films on glass is possible using the thermal sublimation deposition method because of its high vapor pressures [15, 16]. The same method is used to manufacture CdTe films on glass [17, 18]. Another reason rapid thermal deposition is suitable for GeSe is that the common phase impurities of GeSe are $GeSe_2$ and Ge. These impurities' vapor pressure are very low compared to GeSe, so while deposition, the impurities will remain in the boat while the pure GeSe will be deposited [19]. GeSe film has also been deposited using magnetron sputtering. One example is FTO/CdS/GeSe/C–Ag solar cells, which exhibited an efficiency of 0.05% with a J_{sc}, V_{oc}, and fill factor (FF) of 0.85 mA cm^{-2}, 220 mV, and 26.50%, respectively [20]. The important parameter of GeSe that makes it a potential absorber material for a solar PV application is its bang gap which is 1.14 eV [19, 21]. The material GeSe was reported as back as in the 1950s [22]. Its high potential in optoelectronics is also not new. People have known its potential even in the 1960s [7]. Despite this, developing the first experimental data of a GeSe-based solar cell was done only in 2017. They managed to achieve an efficiency of 1.48% [19]. The most recent developments, along with their timeline, are beautifully reported by the Mathew J. Smiles group [23, 24]. The efficiency of GeSe solar cells keeps getting higher and higher every time it gets reported. For example, glass/Mo/GeSe/CdS/iZO/ITO/Ag cell showed an efficiency of 3.1% along with $V_{OC} = 0.33$ V, $J_{SC} = 20.1$ mA cm^{-2}, and FF = 47.1%, which was already twice the previously best-reported efficiency of superstrate GeSe solar cell [25]. Later surface passivated GeSe films showed to an efficiency of 5.2% along with $V_{OC} = 0.36$ V, $J_{SC} = 26.9$ mA cm^{-2}, and FF = 54% which was even higher [26]. In the present work, we used solar cell capacitance simulator (SCAPS) software to optimize the absorber and buffer layer of a generic GeSe-based solar cell, and also discussed some data conflicts in the literature for GeSe. Along with the investigation of experiment-based setback while preparing solar cell based on superstrate configuration and its solution, this work explains in the simplest way possible, the physics behind introducing hole transport layers (HTLs) in solar cells.

2. Device Structure and Simulation Parameters (Experimental)

2.1. Device Structure and Configuration. A simple solar cell is just a P–N junction in no bias configuration where the generation of electron–hole pair takes place due to the incident photon in the P-type layer of the junction, usually called the absorber layer. In this work, for the absorber layer, GeSe is used, and for the N-type layer, which is sometimes called the buffer layer, we used cadmium sulfide (CdS), one of the standard buffer layers. CdS consist of toxic constituents, compared with N-type silicon, a nontoxic buffer layer for the second configuration. The general configuration of this simple solar cell is taken as front contact/ITO/buffer layer/GeSe/back contact, as shown in Figure 1(a), along with its equivalent circuit in Figure 1(b). The indium tin oxide (ITO) is coated on the glass through which the sunlight enters. Due to illumination from the sun or any light source, an ideal diode generates a potential difference, namely, open circuit voltage (V_{oc}). The potential difference can be represented as if the N-type is grounded and the P-type is connected to a voltage source.

2.2. Simulation Parameters. SCAPS, a magnificent one-dimensional software, is developed by Mr. Marc Burgelman of the University of Gent, Belgium [27]. This software was initially designed to analyze CdTe and $CuInSe_2$ solar cells [28, 29]. Now the software has seen many improvements to simulate almost all crystalline and amorphous solar cell families [26, 29–31]. SCAPS provides consistent results with computational and experimental work [32]. It stimulates the solar cell by solving semiconductor equations. Many dignitary researchers like Koen Decock, Stefaan Degrave, and Alex Niemegeers have influenced the development of SCAPS [28, 33]. In the present study, SCAPS has been been used to optimize the conditions to achieve he best possible solar cell using GeSe as an absorber layer. Usually, in SCAPS, the simulation is done under certain conditions; those conditions can be saved for future simulations in an action list [34]. The temperature is set to be at 300 K, which falls around the colder value of the room temperature. Ideally, the temperature on the rooftops is higher than this. The sun simulation is taken from the default spectra file of SCAPS named "AM1_5G 1 sun."

The intended solar cell is designed in SCAPS according to Figure 1(a), and configurated using the parameters tabulated in Table 1. One of the off-putting points about simulation is that it often deviates from the experimental data. Still, SCAPS allows us to figure out that deviation by including the defect parameter option available in the SCAPS software. Studying the effect of defects is crucial because producing an ideal film without defects is as much an art as science [43]. Table 2 shows the defect parameters of the constituent layer from the literature as it is necessary for the practicality and novelty of our simulation.

3. Results and Discussion

3.1. Optimization of the Absorber Layer. The absorber layer's thickness is optimized against the four critical I–V characteristics: open circuit voltage (V_{oc}), short circuit current density (J_{sc}), efficiency (η), and FF by using the batch setup and recorder setup options for both buffer layer configurations (ITO/CdS/GeSe and ITO/n-Si/GeSe). The parameters except FF seem to saturate with an increase in thickness, as shown in Figure 2(a)–2(d). J_{sc} can be represented as follows [46]:

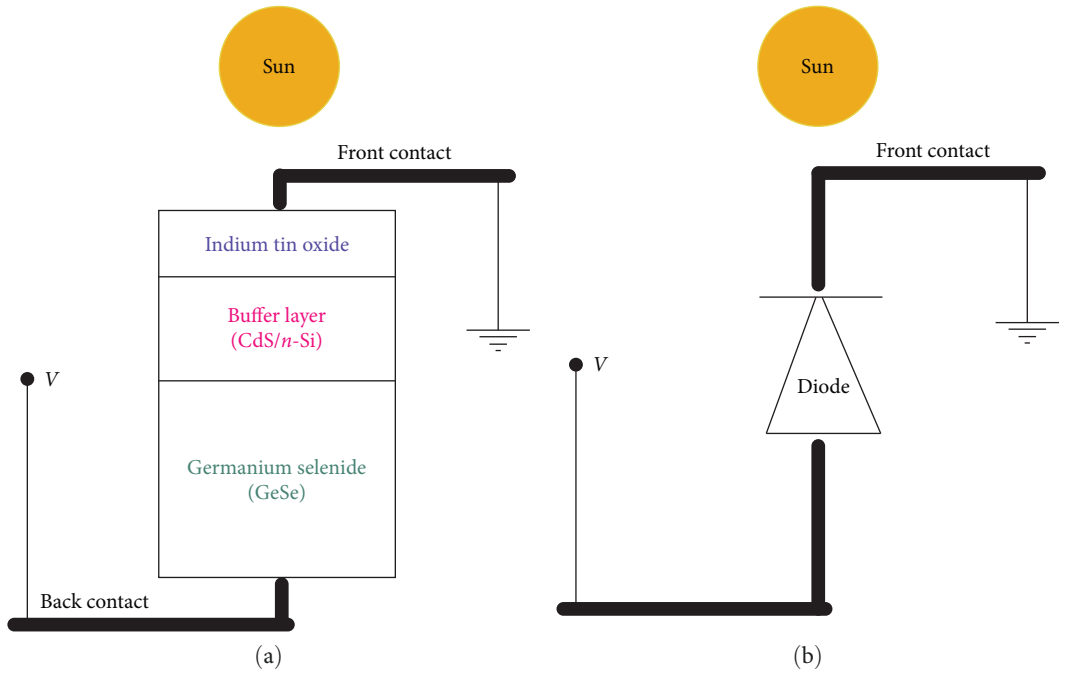

Figure 1: Schematic of (a) simple solar cell and (b) an equivalent diode circuit of the solar cell.

Table 1: SCAPS parameters used in the simulation with the respective references.

	CdS [35]	GeSe [13, 36]	*n*-Si [37–40]	ITO [41]
Bandgap (eV)	2.42	1.14 [13]	1.2 [37]	3.5
Electron affinity (eV)	4.5	4.07 [42]	4 [38]	4.6
Di. permittivity	9	15.3 [13]	9.8 [39]	8.9
CB eDOS (cm^{-3})	2.2×10^{18}	4×10^{18} [36]	2.58×10^{16} [38]	2.2×10^{18}
VB eDOS (cm^{-3})	1.8×10^{19}	1.75×10^{19} [36]	2.65×10^{16} [38]	1.8×10^{19}
Electron thermal velocity ($cm\,s^{-1}$)	2.6×10^{7}	1×10^{7} [36]	1×10^{7}	1×10^{7}
Hole thermal velocity ($cm\,s^{-1}$)	1.3×10^{7}	1×10^{7} [36]	1×10^{7}	1×10^{7}
Electron mobility ($cm^2\,V^{-1}\,s^{-1}$)	3.4×10^{2}	1.27×10^{1} [13]	45 [38]	10
Hole mobility ($cm^2\,V^{-1}\,s^{-1}$)	1×10^{1}	1.12×10^{1} [13]	47 [38]	10
Shallow donor density (cm^{-3})	3×10^{16}	0 [36]	7×10^{20} [40]	1×10^{21}
Shallow acceptor density (cm^{-3})	0	1×10^{16} [36]	0 [38]	0

Table 2: Defects parameters of the constituent layer.

Defect type	ITO [41] Neutral	CdS, Defect 1 [35] Neutral	CdS, Defect 2 [35] Single acceptor	GeSe [44] Single donor	*n*-Si [45] Neutral
Capture cross-section electrons (cm^2)	1×10^{-17}	1×10^{-12}	1×10^{-20}	1×10^{-15}	1×10^{-14}
Capture cross-section holes (cm^2)	1×10^{-15}	1×10^{-12}	1×10^{-11}	1×10^{-17}	1×10^{-14}
Total defect density (cm^{-2})	1×10^{16}	1×10^{18}	2.9×10^{16}	1×10^{13}	1×10^{16}

$$J_{SC} = eG(d_h + d_e). \quad (1)$$

The short circuit current density depends on the electronic charge (e), carrier generation rate (G), and diffusion lengths of holes (d_h) and electrons (d_e). d_h, d_e, and charge on an electron cannot change, but the carrier generation rate, which is a function of the absorption coefficient and thickness of the material, changes. Even if it changes, the generation rate will have an upper limit depending on the material's carrier concentration per unit area, recombination data, etc. This saturation limit leads the J_{sc} to saturate (Figure 2(c)) [47].

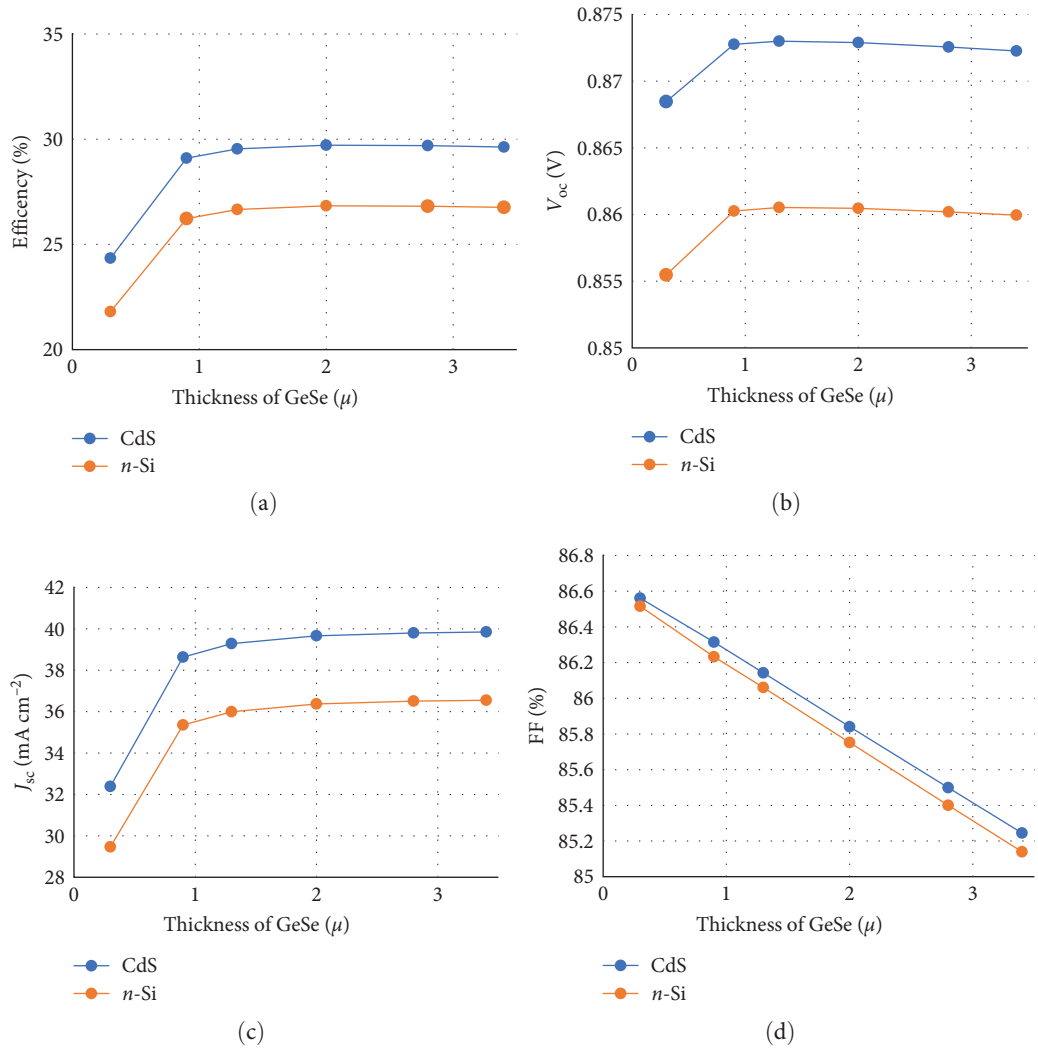

FIGURE 2: Variation of (a) efficiency (η), (b) open-circuit voltage (V_{oc}), (c) J_{sc}, and (d) fill factor (FF) versus thickness of GeSe layer.

$$V_{oc} = \frac{KT}{e} \ln\left(\frac{J_{sc}}{J_v}\right). \quad (2)$$

Now the open current voltage is a function of Boltzmann constant (K), temperature (T), electronic charge (e), J_{sc}, and J_v. J_v is the volume recombination current density. Usually, J_{sc} is weaker than J_v [47], so the value $\ln(J_{sc}/J_v)$ also becomes almost a constant which makes the V_{oc} also constant, as shown in Figure 2(b). The FF is heavily affected by the internal electric field [48] when the thickness increases, the internal electric field reduces and gets deformed, making the FF reduce with an increase in thickness [46, 48].

$$\eta = \frac{(V_{oc} I_{sc} \mathrm{FF})}{P_{in}}. \quad (3)$$

Even though the efficiency here depends on a decreasing FF, the change in FF for thickness is not comparable with the input power from in the sun (P_{in}), thus making efficiency (η) also a reasonably constant value at a larger thickness value as in Figure 2(a). The thickness value between 2 and 3 μm gives the best results. Thus, we chose 2 μm as the optimized value of the absorber layer. Excellent device performance was achieved at this value, and the related I–V parameters are tabulated in Table 3. The buffer layer's unoptimized thickness is 0.5 μm, and the thickness of standard ITO, which is 0.2 μm, is used.

TABLE 3: I–V characteristics for 2 μm of GeSe-based structure for different buffer layers.

Buffer layers	V_{oc} (V)	J_{sc} (mA cm^{-2})	FF (%)	H (%)
CdS	0.8699	35.47	85.84	26.49
n-Si	0.8605	36.37	85.74	26.84

The back contact is connected near the depletion layer when the absorber layer is thin, especially in a TFPV. The photons absorbed away from the surface will probably recombine immediately into the back contact recombination current [30, 32]. If the absorber layer is too long, the generated carrier might not have a long enough lifetime to contribute to the diode's forward current [30, 31]. Comparing

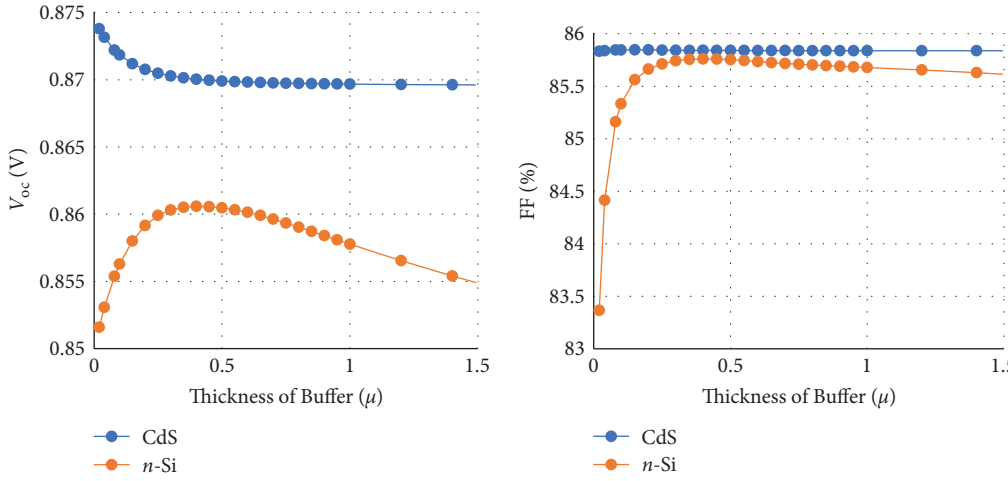

Figure 3: Variation of (a) V_{oc} and (b) fill factor versus thickness of buffer layer.

Table 4: I–V parameters after optimization of the buffer layer.

Buffer layers (μm)	V_{oc} (V)	J_{sc} (mA cm^{-2})	FF (%)	H (%)
CdS, 0.05	0.8724	38.975	85.84	29.19
n-Si, 0.4	0.8606	37.28	85.76	27.52

Table 5: Fluctuating parameters and their respective references.

Fluctuating parameter	Fluctuating values with references
Bandgap (eV)	1.075 [52], 1.14 [13], 1.25 [53], 1.45 [47, 48], 1.53 [7]
Electron affinity (eV)	4.07 [42], 3.2 [54], 3.8 [55]

the mobility of electrons and that of the hole, we need a thicker absorber layer when compared to the buffer layer because the carriers of each layer could reach the respective electrodes at approximately the same time [13, 49].

3.2. Optimization of the Buffer Layer. After optimizing the absorber layer by fixing an arbitrary thickness of 0.5 μm for the buffer layer, the buffer layer parameters were optimized. The smaller the thickness of the buffer layer, the better the solar cell's performance, but it should not be too small compared to the depletion layer of the P–N diode. The thinnest and most economically advantageous thickness for CdS is 0.05 μm, used by many researchers [50]. In the case of the n-Si layer, it follows similar graphs of CdS results, but there is a local maximum in V_{oc} and FF graphs before reaching the lowest value, as shown in Figures 3(a) and 3(b). For the n-Si layer, the best performance is achieved when the thickness of the layer is set at 0.4 μm. The final I–V parameters after optimizing the absorber and buffer layers are tabulated in Table 4. Ideally, the thickness of the buffer layer must be less than the diffusion length of the holes of the absorber layer so that it might reach the metal electrode without recombining [49]. It is how thin absorber layers maximize the current flow [51].

When comparing Tables 3 and 4, we can say that a significant change occurred once we optimized the buffer layer.

3.3. Contradictory Values of Parameters. In the literature, there are many values in a particular range for some parameters of GeSe. In other words, GeSe seems to have many different values for a single parameter like bandgap, relative dielectric permittivity, electron affinity, etc. The value fluctuation may result from preparation methods, various experimental methods, or other reasons. If someone prepares GeSe in a laboratory, it might have one of these values or even lie in this range of values. This section will address the issue of how the fluctuation of specific parameters can affect the cell's performance. The experimental fluctuation of values is listed in Table 5, along with references.

These bandgap data contain both direct and indirect bandgap values. The effect of dielectric permittivity does change the result but only a negligible amount, so it is not discussed here. Still, the impact of bandgap and electron affinity is considerable.

The change in I–V parameters due to the change in electron affinity does saturate after a value in some cases (Figures 4(b) and 4(c)). In other cases, it does not seem to influence that much (Figures 4(a) and 4(d)). The bandgap does produce a whooping change in the intended range in all I–V parameters. So, these values of the parameters can be optimized if the cause of the fluctuation is known. This kind of optimization while preparing is required for a newbie absorber layer like GeSe to make it a commercially successful absorber layer for TFPVs.

3.4. Low Interface Defect Technique. Now, the important layers of the P–N junction solar cell are optimized using SCAPS. The development of the first experimental data of a GeSe-based solar cell was reported only in 2017. They achieved an efficiency of 1.48% [19] of configuration glass/ITO/GeSe/CdS/Au. This value is not even comparable with the simulated value due to high defect configuration, which may have resulted from microcracking, native oxide

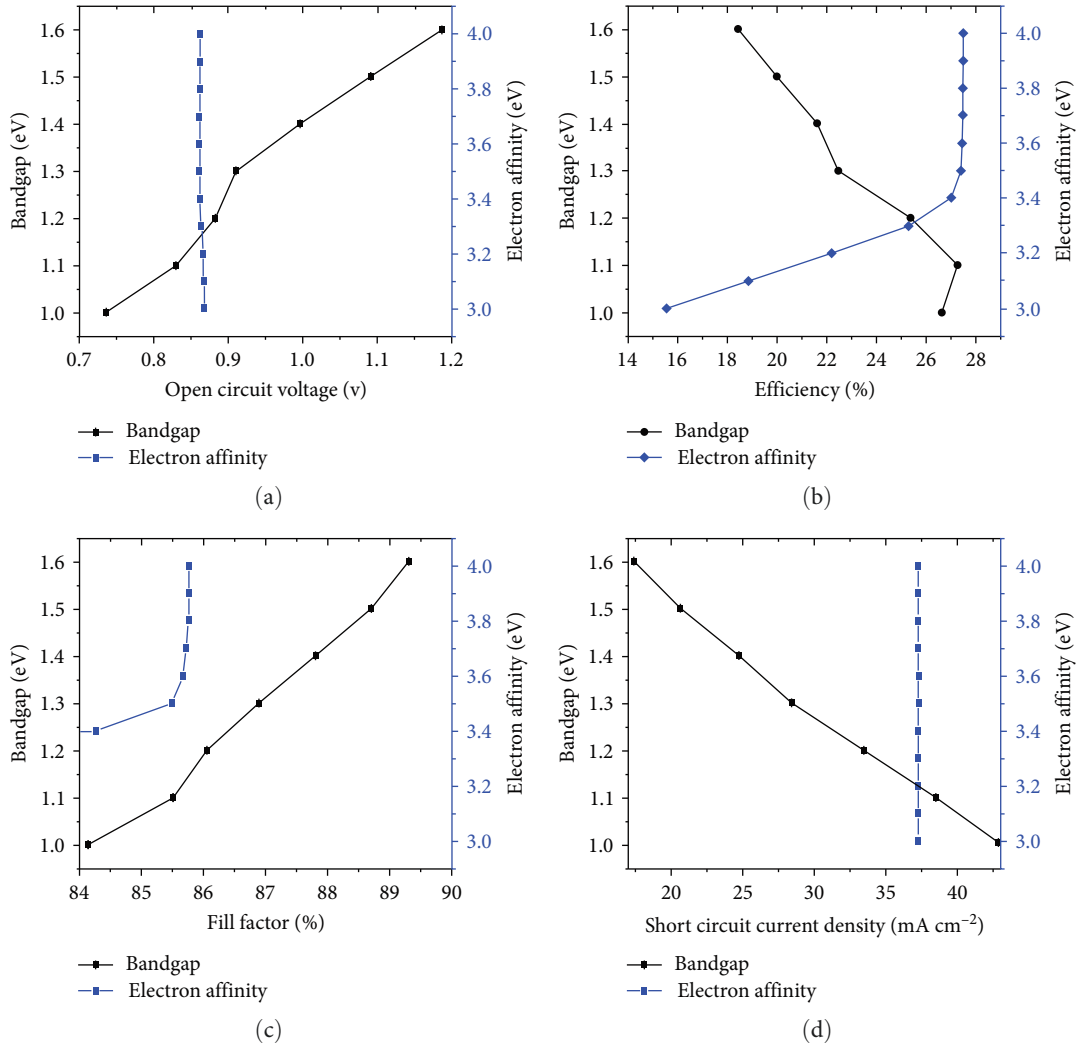

FIGURE 4: Variation of (a) V_{oc}, (b) η, (c) FF, and (d) J_{sc} with bandgap and electron affinity.

formation, antisite defects, etc. GeSe is only a recently developed functional material, so many techniques exist to enhance its performance. Like selenization of the GeSe absorber layer, etching of the absorber layer to enhance the absorbance, determining the best annealing temperature, change in configuration design, etc. One of the design improvements GeSe can take is that it should undergo a substrate configuration instead of a simple superstrate configuration. In other words, the deposition of CdS must be on GeSe and not the opposite. Most of the GeSe cells that have been reported are of superstrate configuration, as shown in Figure 5(b) [56, 57].

Deposition of the GeSe on a buffer layer requires a higher temperature, like 550°C [24, 58, 59], even though the crystallization temperature of GeSe is about 300°C [60]. This high-temperature treatment might lead to diffusion of the buffer layer constituents into the absorber layer, eventually leading to deep defects [25]. When the cell is prepared in substrate configuration, as shown in Figure 5(a), the deposition can be done in low-temperature methods like sputtering, chemical bath deposition, etc. [61]. It is how we can avoid annealing the absorber layer and the buffer layer. Whether this deep defect, which arose from annealing, leads to the low performance of the device built is not yet [25]. However, SCAPS allows us to find if the deep defects can have such an influence. Thus, the device efficiency against the interface defect density of the GeSe/CdS interface in superstrate configuration is analyzed, as shown in Figure 5(b). It was done using the same structure mentioned by Xue et al. [19], hoping to get results similar to that of the first experimental data of the GeSe-based solar cell developed in 2017. The results are given in Figure 6 and Table 6.

The results show that the simulated efficiency and FF are close to the experimental value, as shown in Figure 7.

Still, the V_{oc} and J_{sc} are not comparable to the experimental value, so by looking at the results, we can safely say that diffusion of buffer layer constituents may not be the only reason for the deviated value. However, the efficiency is heavily affected by this (Figure 6). Thus, tackling this problem by adopting substrate configuration will experimentally lead to better results. Many other experimental techniques for the improvement of GeSe-based solar cells are well described by Liu et al. [6].

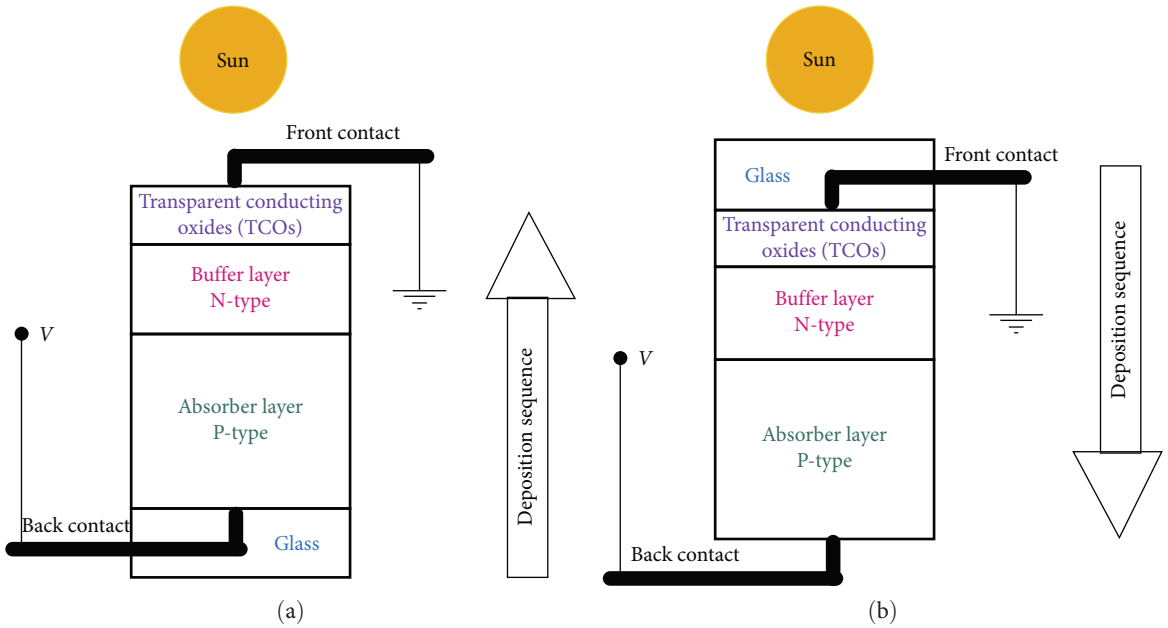

Figure 5: (a) Substrate and (b) superstrate configuration of the cell.

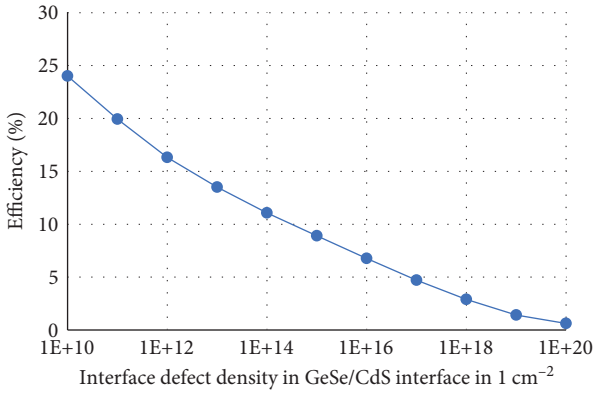

Figure 6: Efficiency versus interface defect density plot for GeSe/CdS.

Table 6: The *I–V* parameters of the first GeSe solar cell in 2017.

I–V parameters	Values [19]
V_{oc} (*V*)	0.24
J_{sc} (mA cm^{-2})	14.48
FF (%)	42.60
H (%)	1.48

3.5. Role of Hole Transport Layer. To improve the cell's performance further, we must analyze the energy band diagram of our cell. Figure 8(a) represents the energy band diagram of our optimized layers along with its bandgap. The ITO/CdS/GeSe configuration has a V_{oc} of 0.87 eV, as in Table 4. When the V_{oc} of the cell is significantly less than the bandgap of the absorber used, we can say that significant recombination dominates the V_{oc} and J_{sc}.

Suspecting that this recombination happens in the metal–GeSe junction at the back of the cell, we can analyze the band bending before and after reaching equilibrium during the junction formation. The metal–GeSe junction is diagrammatically represented in Figure 9. This metal–semiconductor contact must be rectifying or ohmic. Rectifying contact forms a Schottky barrier/Schottky diode [62, 63]. The conditions for forming a Schottky barrier differ based on the semiconductor type, P or N [62, 63], which are tabulated in Table 7. W_m is the work function of the metal used, and W_{sc} is the work function of the semiconductor. For P-type semiconductors, ohmic contact is a hole-allowing contact, and rectifying contact is a hole-blocking contact [63, 64].

The Fermi level of the GeSe is lower than that of the metal, as in Figure 9(a). When the junction is set, the Fermi level of both materials gets aligned. There is a transfer of electrons from the metal to the semiconductor until the equilibrium is reached. The semiconductor bands must bend in the downward direction, thus forming a rectifying contact [63, 65]. The initial Fermi level (green) is below the final Fermi level (purple), as shown in Figure 9(b). The usual *IV* curve of a solar cell will show a negative current for an appreciable positive voltage. The current flows from the semiconductor to the metal, so the electron must flow in the opposite direction. As the name of the contact suggests hole blocking contact, the downward bending of the bands prohibits quite a few electrons with lower energy from entering the valance region of the semiconductor, as described in Figure 9(b). Thus, the holes are unable to enter the valance region of the metal. It happens purely because of the shape of the bending of the semiconductor bands. Thus, the rejected holes recombine with the minority carriers (electrons) in the P-type material. These holes could

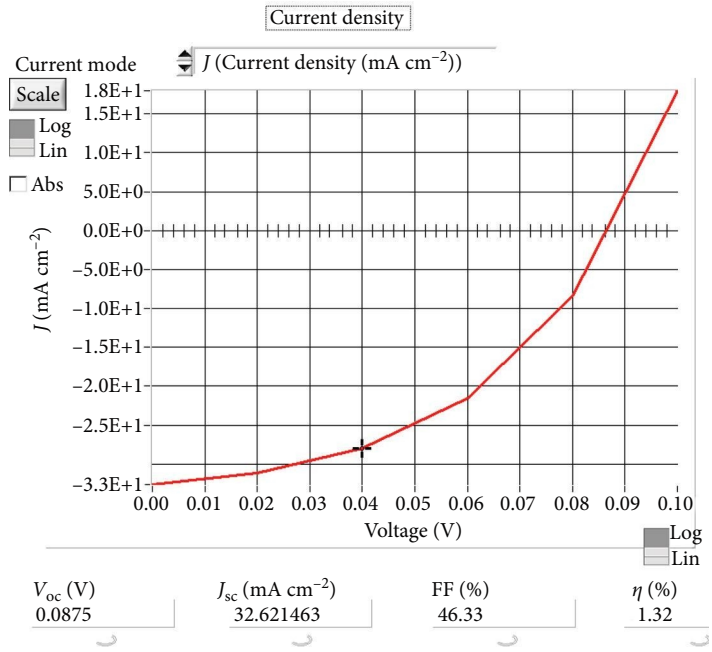

FIGURE 7: I–V parameters of glass/ITO/GeSe/CdS/Au with IF defect density of 5.5×10^{18} cm^{-2} in GeSe/CdS.

have been harvested to increase the cell's performance, contributing to bulk recombination. To tackle this, we introduce a thin layer of P^+-type material which is, in our case, cuprous oxide (Cu_2O), a HTL. HTLs have higher acceptor density, which makes our solar cell into a P^+PN structure instead of an ordinary P–N junction. Since we are putting this layer between the back contact and the absorber layer, this layer is also called a back surface field layer. The band energy diagram after inserting the HTL layer is given in Figure 8(b).

We again need to analyze the metal–P^+ junction to understand hole the HTL layer makes a difference. We can see that the Fermi level of the P^+-type layer is higher than that of the metal, as shown in Figure 10(a). So, during alignment to match the Fermi levels, the bands must bend up this time. We can see that the initial Fermi level (red) is above the final Fermi level (purple) in Figure 10(b). The upward bending of the band allows even the lower energy electrons to enter the valance region of the semiconductor. It again happens because of the shape of the bending of the semiconductor conduction bands. Thus, the electrons and holes are saved from recombination, increasing the cell's performance instead of contributing to bulk recombination. We used cuprous oxide as HTL in ITO/CdS/GeSe and ITO/n-Si/GeSe to compare its performance by analyzing its I–V curves, as shown in Figure 11 and Table 8. The parameters used for the simulation of the Cu_2O layer was obtained from reference [66].

The n-Si and CdS buffer layer cell structures with no HTL are similar. There is much improvement as we added the back surface layer to our existing structure. The V_{oc} of the ITO/CdS/GeSe/Cu_2O configuration is the only one that is approximately equal to the bandgap of the absorber. Hence, it means that there was dominant recombination due to bulk recombination in the ITO/CdS/GeSe configuration, which has been reduced by introducing an HTL. There is an improvement in J_{sc} in the case of CdS buffer cells but not in n-Si buffer cells. The efficiency of both buffer cells has seen improvement.

The work based on GeSe solar cells is compared with other experimental and theoretical results, as shown in Table 9.

3.6. Temperature Effect on the I–V Parameters and Stability Comparison. As discussed in the Introduction section, the rooftops where the solar panels are usually placed are not 300 K. In an average tropical country, the temperature ranges from 295 to 308 K. Thus, we also optimized the effect of temperature on the performance of the I–V parameters, as shown in Figure 12(a)–12(d).

All the parameters get slightly decreased with an increase in temperature except for J_{sc}. Since the absorber layer is a semiconductor, the conductivity increases with the temperature. All the increases and decreases of the I–V parameters are not very dominant in the plots. Thus, the typical natural temperature range would not affect the device's performance much. All these characteristics are in much so favor of proving that GeSe-based thin film solar cells are worthy of investing our time and money in. Another important reason why GeSe is worthy enough is its stability. There is a good amount of evidence to attribute this stability to the Ge (4s) and Se (4p) bonding [26, 70]. The stability is enough to be approved by the IEC following the code IEC 61646 used for the thin film solar cells commercialization [26, 71]. Here are some existing data that have proven the stability of GeSe engineered in different configurations of solar cells. These solar

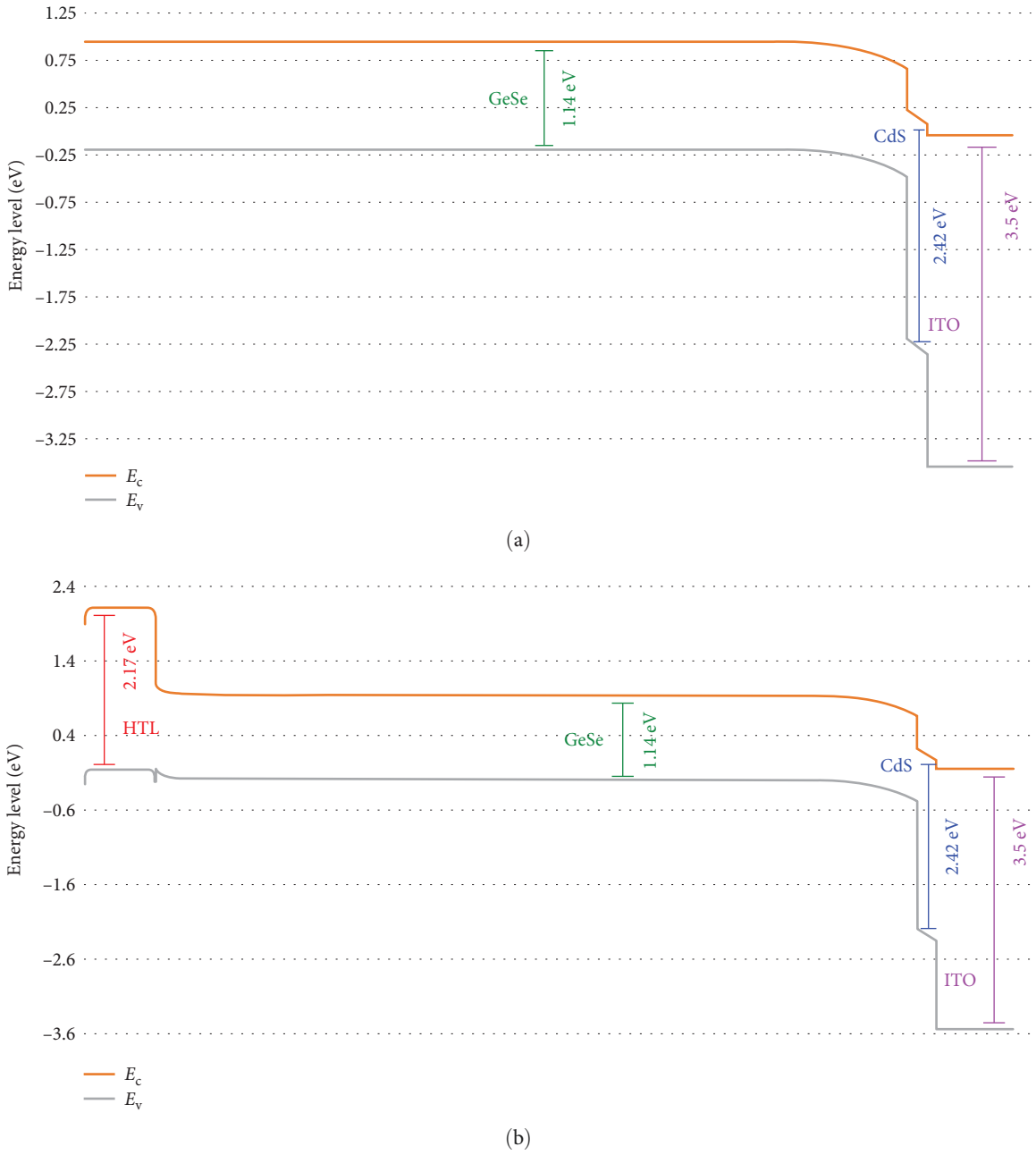

FIGURE 8: Band energy diagram of (a) ITO/CdS/GeSe and (b) ITO/CdS/GeSe/Cu_2O, obtained from SCAPS simulation of this work.

cells had no encapsulation during the stability measurements (Table 10).

4. Conclusion

TFPVs are better than Si-based solar cells in terms of cost. We choose GeSe for this particular paper because of its earth's abundance, nontoxic constituents, and optimal absorption coefficient for thin film PVs. The optimal thickness of GeSe was 0.2 μm for ITO/CdS/GeSe and ITO/n-Si/GeSe configurations. The I–V parameter of ITO/CdS/GeSe came up to be PCE = 26.49%, $V_{OC} = 0.8699$ V, $J_{SC} = 35.47$ mA cm^{-2}, FF = 85.84%, and of ITO/n-Si/GeSe came up to be PCE = 26.84%, $V_{OC} = 0.8605$ V, $J_{SC} = 36.37$ mA cm^{-2}, and FF = 85.74%. Optimization of the buffer layers (CdS—0.05 μm, n-Si—0.4 μm) led to an increment in the cell's performance. We also saw that the fluctuation of the bandgap is far more concerning than the fluctuation of electron affinities because the change in electron affinity affects the efficiency and FF of the cell but up to a limit.

In contrast, the change in bandgap affects all the I–V parameters very much. Switching to a substrate configuration

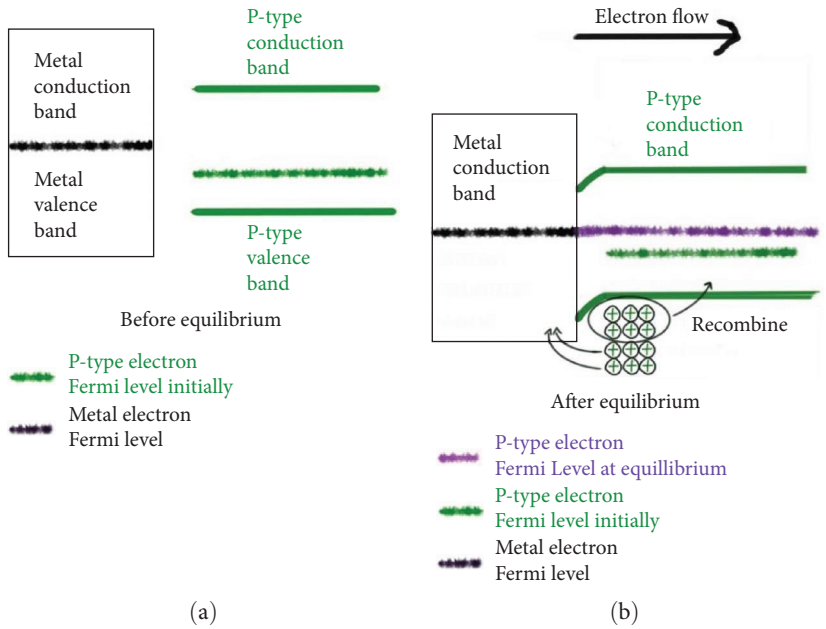

Figure 9: Metal-P-type contact: (a) before reaching equilibrium; (b) after reaching equilibrium [63, 65].

Table 7: Ohmic and rectifying contact conditions.

Semiconductor type	Rectifying contact	Ohmic contact
P-type	$W_m < W_{sc}$	$W_m > W_{sc}$
N-type	$W_m > W_{sc}$	$W_m < W_{sc}$

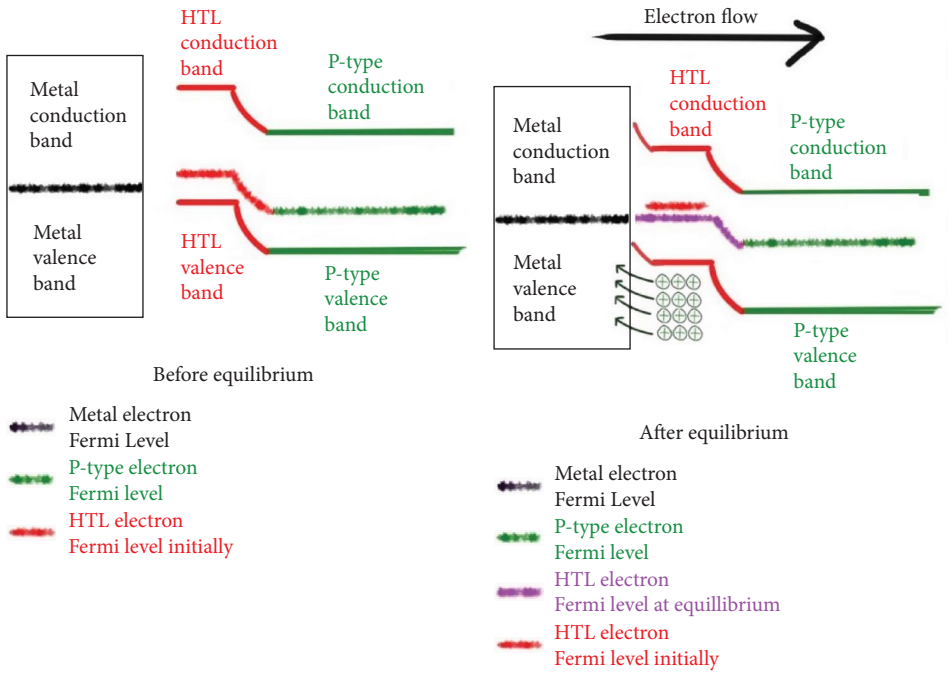

Figure 10: Metal-P^+-type contact: (a) before reaching equilibrium; (b) after reaching equilibrium.

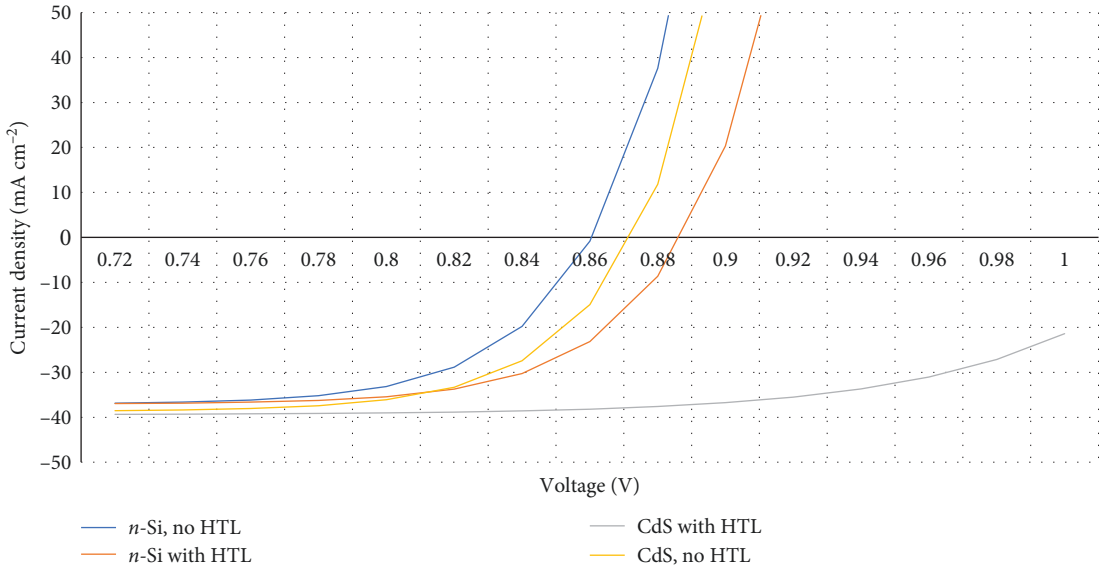

Figure 11: I–V curves of n-Si and CdS buffer solar cells with and without HTL.

Table 8: I–V parameters of with and without HTL configurations.

Configuration	V_{oc} (V)	J_{sc} (mA cm^{-2})	FF (%)	H (%)
ITO/CdS/GeSe	0.87	38.97	85.84	29.19
ITO/CdS/GeSe/Cu_2O	1.04	39.66	80.23	33.12
ITO/n-Si/GeSe	0.86	37.28	85.76	27.52
ITO/n-Si/GeSe/Cu_2O	0.88	37.28	85.84	28.39

Table 9: Comparison with other theoretical and experimental results.

Ref.	Configuration	V_{oc} (V)	J_{sc} (mA cm^{-2})	FF (%)	η (%)
[19]	ITO/CdS/GeSe	0.24	14.48	42.6	1.48
[25]	ITO/CdS/GeSe	0.33	20.1	47.1	3.1
[67]	FTO/CdS/p-GeSe/Au	0.135	12.61	38.2	0.65
[68]	ZnSe/GeSe/WSe_2	1.07	47.84	82.80	42.18
[69]	AZO/i-ZnO/CdS/GeSe/NiO/Au	0.903	39.79	87.28	31.37
This work	ITO/CdS/GeSe/Cu_2O	1.04	39.66	80.23	33.12

from a superstrate configuration is essential as the simulation proved that the diffusion-caused interface defect density would drag the efficiency at an alarming rate. The introduction of the HTL layer boosted the performance of all the configurations of GeSe solar cells. A notable increase happened with ITO/CdS/GeSe when the Cu_2O was included to make it ITO/CdS/GeSe/Cu_2O the V_{oc} increased from 0.87 to 1.04 V. The J_{sc} increased from 38.97 to 39.66 mA cm^{-2}, and the efficiency rose from 29.19% to 33.12%. The FF was slightly decreased instead of increase in this particular configuration. The logic behind introducing the HTL relies on the band bending while forming the contact was discussed well. The average temperature range of a tropical country (295–308 K) does not influence the solar cell in great lengths simulation-wise. This theoretical paper aims to back up the statement, "GeSe-based PV panels are a very fair option for Green energy generation, and with enough research time and budget, it can potentially be the best option for green energy generation."

Data Availability

Data will be made available upon valid request.

Conflicts of Interest

The authors declare that they have no conflicts of interest.

Authors' Contributions

A. Bala Sairam: data curation, writing an original draft; Yogesh Singh: writing review and editing; Mamta: writing, review and editing; V. N. Singh: supervision, review, and

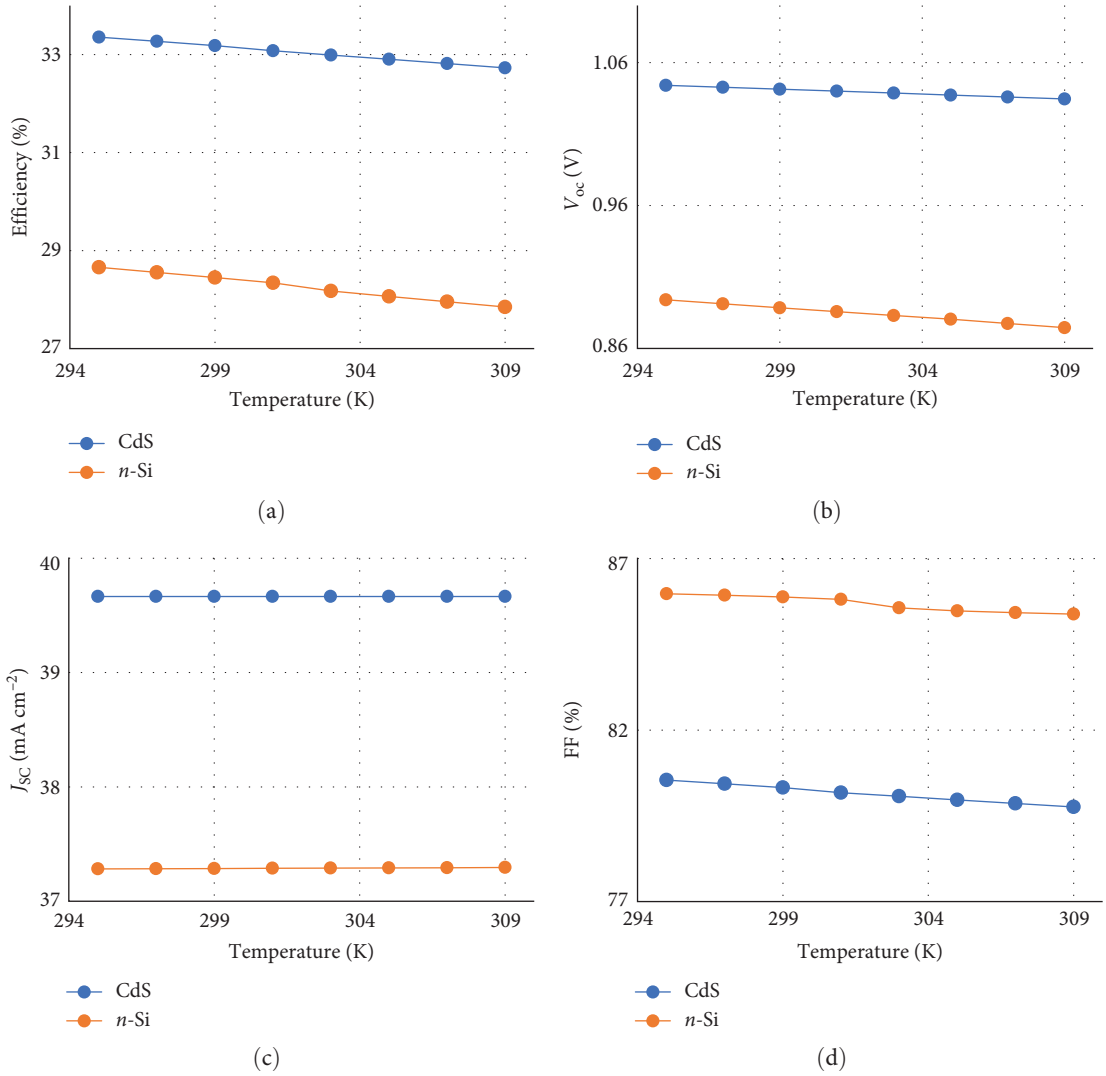

Figure 12: Impact of temperature on the (a) η, (b) V_{oc}, (c) J_{sc}, and (d) FF.

Table 10: Stability comparison of GeSe solar cells.

Ref.	Configuration	Duration	Eta
[19]	ITO/CdS/GeSe/Au	6 weeks	No obvious degradation
[70]	FTO/SnO_2/GeSe/Au	7,000 s	No obvious degradation
[70]	FTO/SnO_2/GeSe/Au (air stability)	30 days	Slight improvement
[70]	FTO/CdS/GeSe/Au (air stability)	30 days	Reduced to half
[26]	ITO/CdS/Sb_2Se_3/GeSe/Au	12 months	No efficiency loss

editing. Yogesh Singh and Mamta contributed equally to this work.

Funding

We thank the Indian Academy of Sciences (IAS), Bengaluru, for providing a stipend under the Summer Research Fellowship (SRF) 2022.

Acknowledgments

We thank Professor Burgelman of Gent University, Belgium, for providing the SCAPS program.

References

[1] M. Taguchi, A. Yano, S. Tohoda et al., "24.7% record efficiency HIT solar cell on thin silicon wafer," *IEEE Journal of Photovoltaics*, vol. 4, no. 1, pp. 96–99, 2014.

[2] D. C. Jordan and S. R. Kurtz, "Photovoltaic degradation rates —an analytical review," *Progress in Photovoltaics*, vol. 21, no. 1, pp. 12–29, 2013.

[3] P. J. Collings, "Simple measurement of the band gap in silicon and germanium," *American Journal of Physics*, vol. 48, no. 3, pp. 197–199, 1980.

[4] M. A. Green and M. J. Keevers, "Optical properties of intrinsic silicon at 300 K," *Progress in Photovoltaics*, vol. 3, no. 3, pp. 189–192, 1995.

[5] M. A. Green, "Self-consistent optical parameters of intrinsic silicon at 300 K including temperature coefficients," *Solar Energy Materials and Solar Cells*, vol. 92, no. 11, pp. 1305–1310, 2008.

[6] S.-C. Liu, Y. Yang, Z. Li, D.-J. Xue, and J.-S. Hu, "GeSe thin-film solar cells," *Materials Chemistry Frontiers*, vol. 4, no. 3, pp. 775–787, 2020.

[7] C. R. Kannewurf and R. J. Cashman, "Optical absorption and photoconductivity in germanium selenide," *Journal of Physics and Chemistry of Solids*, vol. 22, pp. 293–298, 1961.

[8] N. L. Muttumthala and A. Yadav, "A concise overview of thin film photovoltaics," *Materials Today: Proceedings*, vol. 64 Part 3, pp. 1475–1478, 2022.

[9] M. Nakamura, K. Yamaguchi, Y. Kimoto, Y. Yasaki, T. Kato, and H. Sugimoto, "Cd-free Cu (In, Ga)(Se,S)$_2$ thin-film solar cell with record efficiency of 23.35%" *IEEE Journal of Photovoltaics*, vol. 9, no. 6, pp. 1863–1867, 2019.

[10] M. J. Watts, P. Hatton, R. Smith et al., "Chlorine passivation of grain boundaries in cadmium telluride solar cells," *Physical Review Materials*, vol. 5, no. 3, Article ID 035403, 2021.

[11] G. W. C. Kaye and T. H. Laby, *Tables of Physical and Chemical Constants*, National Physical Laboratory, United States, 15th edition, 1986.

[12] B. Mukherjee, Y. Cai, H. R. Tan, Y. P. Feng, E. S. Tok, and C. H. Sow, "NIR Schottky photodetectors based on individual single-crystalline GeSe nanosheet," *ACS Applied Materials and Interfaces*, vol. 5, no. 19, pp. 9594–9604, 2013.

[13] S.-C. Liu, Y. Mi, D.-J. Xue et al., "Investigation of physical and electronic properties of GeSe for photovoltaic applications," *Advanced Electronic Materials*, vol. 3, no. 11, Article ID 1700141, 2017.

[14] Y. Lv, L. Yang, J. Zhang, J. Wu, H. Wu, and X. Xu, "Enhanced performance of GeSe thin-film solar cells via bifacial charge transport materials design," *Vacuum*, vol. 201, Article ID 111119, 2022.

[15] E. A. Irene and H. Wiedemeier, "The sublimation kinetics of GeSe single crystals," *Zeitschrift für Anorganische und Allgemeine Chemie*, vol. 411, no. 2, pp. 182–192, 1975.

[16] H. Ipser, M. Gambino, and W. Schuster, "The germanium-selenium phase diagram," *Monatshefte für Chemie - Chemical Monthly*, vol. 113, no. 4, pp. 389–398, 1982.

[17] B. L. Williams, A. A. Taylor, B. G. Mendis et al., "Core-shell ITO/ZnO/CdS/CdTe nanowire solar cells," *Applied Physics Letters*, vol. 104, no. 5, Article ID 53907, 2014.

[18] J. D. Major, R. E. Treharne, L. J. Phillips, and K. Durose, "A low-cost nontoxic post-growth activation step for CdTe solar cells," *Nature*, vol. 511, no. 7509, pp. 334–337, 2014.

[19] D.-J. Xue, S.-C. Liu, C.-M. Dai et al., "GeSe thin-film solar cells fabricated by self-regulated rapid thermal sublimation," *Journal of the American Chemical Society*, vol. 139, no. 2, pp. 958–965, 2017.

[20] B. Chen, G. Chen, W. Wang et al., "Magnetron sputtering deposition of GeSe thin films for solar cells," *Solar Energy*, vol. 176, pp. 98–103, 2018.

[21] X. Wang, Y. Li, L. Huang et al., "Short-wave near-infrared linear dichroism of two-dimensional germanium selenide," *Journal of the American Chemical Society*, vol. 139, no. 42, pp. 14976–14982, 2017.

[22] A. Okazaki, "The crystal structure of germanium selenide GeSe," *Journal of the Physical Society of Japan*, vol. 13, no. 10, pp. 1151–1155, 1958.

[23] M. J. Smiles, T. P. Shalvey, L. Thomas et al., "GeSe photovoltaics: doping, interfacial layer and devices," *Faraday Discussions*, vol. 239, pp. 250–262, 2022.

[24] D. Shin, B. Saparov, and D. B. Mitzi, "Defect engineering in multinary earth-abundant chalcogenide photovoltaic materials," *Advanced Energy Materials*, vol. 7, no. 11, Article ID 1602366, 2017.

[25] S.-C. Liu, Z. Li, J. Wu et al., "Boosting the efficiency of GeSe solar cells by low-temperature treatment of p-n junction," *Science China Materials*, vol. 64, no. 9, pp. 2118–2126, 2021.

[26] S.-C. Liu, C.-M. Dai, Y. Min et al., "An antibonding valence band maximum enables defect-tolerant and stable GeSe photovoltaics," *Nature Communications*, vol. 12, no. 1, Article ID 670, 2021.

[27] S. Degrave, M. Burgelman, and P. Nollet, "Modelling of polycrystalline thin film solar cells: new features in SCAPS version 2.3," in *Proceedings of 3rd World Conference on Photovoltaic Energy Conversion, 2003*, vol. 1, pp. 487–490, , IEEE, Osaka, Japan, May 2003.

[28] M. Burgelman, P. Nollet, and S. Degrave, "Modelling polycrystalline semiconductor solar cells," *Thin Solid Films*, vol. 361-362, pp. 527–532, 2000.

[29] M. Minbashi, A. Ghobadi, M. H. Ehsani, H. Rezagholipour Dizaji, and N. Memarian, "Simulation of high efficiency SnS-based solar cells with SCAPS," *Solar Energy*, vol. 176, pp. 520–525, 2018.

[30] N. Khoshsirat, N. A. M. Yunus, M. N. Hamidon, S. Shafie, and N. Amin, "Analysis of absorber layer properties effect on CIGS solar cell performance using SCAPS," *Optik*, vol. 126, no. 7-8, pp. 681–686, 2015.

[31] U. Mandadapu, S. V. Vedanayakam, and K. Thyagarajan, "Simulation and analysis of lead based perovskite solar cell using SCAPS-1D," *Indian Journal of Science and Technology*, vol. 10, no. 11, pp. 1–8, 2017.

[32] R. K. Yadav, P. S. Pawar, R. Nandi et al., "A qualitative study of SnSe thin film solar cells using SCAPS 1D and comparison with experimental results: a pathway towards 22.69% efficiency," *Solar Energy Materials and Solar Cells*, vol. 244, Article ID 111835, 2022.

[33] M. Burgelman, J. Verschraegen, B. Minnaert, and J. Marlein, "Numerical simulation of thin film solar cells: practical exercises with SCAPS," in *Proceedings of NUMOS (Int. Workshop on Numerical Modelling of Thin Film Solar Cells, Gent (B), Gent*, pp. 357–366, UGent & Academia Press, January 2007.

[34] M. Burgelman, K. Decock, A. Niemegeers, J. Verschraegen, and S. Degrave, *SCAPS Manual Most Recent*, 2021.

[35] M. Burgelman, "Cadmium telluride thin film solar cells: characterization, fabrication and modeling," *Thin Film Solar Cells: Fabrication, Characterization and Applications*, Wiley, 2006.

[36] M. H. Mohammadi, D. Fathi, and M. Eskandari, "NiO@GeSe core–shell nano-rod array as a new hole transfer layer in perovskite solar cells: a numerical study," *Solar Energy*, vol. 204, pp. 200–207, 2020.

[37] J. Gryko, P. F. McMillan, R. F. Marzke et al., "Low-density framework form of crystalline silicon with a wide optical band gap," *Physical Review B*, vol. 62, no. 12, pp. R7707–R7710, 2000.

[38] N. A. Mahammedi, H. Gueffaf, B. Lagoun, and M. Ferhat, "Numerical simulation and optimization of a silicon clathrate-based solar cell n-Si_{136}/p-S_{i2} using SCAPS-1D program," *Optical Materials*, vol. 107, Article ID 110043, 2020.

[39] X. Blase, "Quasiparticle band structure and screening in silicon and carbon clathrates," *Physical Review B*, vol. 67, no. 3, Article ID 035211, 2003.

[40] A. D. Martinez, L. Krishna, L. L. Baranowski, M. T. Lusk, E. S. Toberer, and A. C. Tamboli, "Synthesis of group IV clathrates for photovoltaics," *IEEE Journal of Photovoltaics*, vol. 3, no. 4, pp. 1305–1310, 2013.

[41] M. A. Rahman, "Design and simulation of a high-performance Cd-free Cu_2SnSe_3 solar cells with SnS electron-blocking hole transport layer and TiO_2 electron transport layer by SCAPS-1D," *SN Applied Sciences*, vol. 3, no. 2, Article ID 253, 2021.

[42] M. J. Smiles, J. M. Skelton, H. Shiel et al., "Ge $4s^2$ lone pairs and band alignments in GeS and GeSe for photovoltaics," *Journal of Materials Chemistry A*, vol. 9, no. 39, pp. 22440–22452, 2021.

[43] F. J. Disalvo, "Solid-state chemistry: a rediscovered chemical frontier," *Science*, vol. 247, no. 4943, pp. 649–655, 1990.

[44] J. Hossain, B. K. Mondal, and S. K. Mostaque, "Computational investigation on the photovoltaic performance of an efficient GeSe-based dual-heterojunction thin film solar cell," *Semiconductor Science and Technology*, vol. 37, Article ID 015008, 2022.

[45] A. Matsuda, "Thin-film silicon—growth process and solar cell application," *Japanese Journal of Applied Physics*, vol. 43, no. 12, pp. 7909–7920, 2004.

[46] S. Dubey, A. S. Mathur, Nidhi, and B. P. Singh, "Effect of defect density in different layers and ambient temperature of n-i-p a-Si single junction solar cells performance," *International Journal of Scientific Research in Physics and Applied Sciences*, vol. 7, no. 2, pp. 93–98, 2019.

[47] R. Brendel and H. J. Queisser, "On the thickness dependence of open circuit voltages of p-n junction solar cells," *Solar Energy Materials and Solar Cells*, vol. 29, no. 4, pp. 397–401, 1993.

[48] M. Stückelberger, A. Shah, J. Krc, M. Despeisse, F. Meillaud, and C. Ballif, "Internal electric field and fill factor of amorphous silicon solar cells," in *2010 35th IEEE Photovoltaic Specialists Conference*, pp. 1569–1574, IEEE, Honolulu, HI, USA, June 2010.

[49] R. T. Mouchou, T. C. Jen, O. T. Laseinde, and K. O. Ukoba, "Numerical simulation and optimization of p-NiO/n-TiO_2 solar cell system using SCAPS," *Materials Today: Proceedings*, vol. 38 Part 2, pp. 835–841, 2021.

[50] J. E. Granata, J. R. Sites, G. Contreras-Puente, and A. D. Compaan, "Effect of CdS thickness on CdS/CdTe quantum efficiency [solar cells]," in *Conference Record of the Twenty Fifth IEEE Photovoltaic Specialists Conference – 1996*, pp. 853–856, IEEE, Washington, DC, USA, May 1996.

[51] T. Glatzel, M. Rusu, S. Sadewasser, and M. C. Lux-Steiner, "Surface photovoltage analysis of thin CdS layers on polycrystalline chalcopyrite absorber layers by Kelvin probe force microscopy," *Nanotechnology*, vol. 19, no. 14, Article ID 145705, 2008.

[52] A. M. Elkorashy, "Indirect forbidden fundamental absorption edge in germanium selenide single crystals," *Physica Status Solidi Basic Solid State Physics*, vol. 135, no. 2, pp. 707–713, 1986.

[53] D. D. Vaughn, R. J. Patel, M. A. Hickner, and R. E. Schaak, "Single-crystal colloidal nanosheets of GeS and GeSe," *Journal of the American Chemical Society*, vol. 132, no. 43, pp. 15170–15172, 2010.

[54] A. M. Afzal, M. Z. Iqbal, S. Mumtaz, and I. Akhtar, "Multifunctional and high-performance GeSe/$PdSe_2$ heterostructure device with a fast photoresponse," *Journal of Materials Chemistry C*, vol. 8, no. 14, pp. 4743–4753, 2020.

[55] Y. Yan, S. Li, J. Du et al., "Reversible half wave rectifier based on 2D InSe/GeSe heterostructure with near-broken band alignment," *Advanced Science*, vol. 8, no. 4, pp. 1–9, 2021.

[56] Y. Zhou, L. Wang, S. Chen et al., "Thin-film Sb_2Se_3 photovoltaics with oriented one-dimensional ribbons and benign grain boundaries," *Nature Photonics*, vol. 9, no. 6, pp. 409–415, 2015.

[57] R. Tang, X. Wang, W. Lian et al., "Hydrothermal deposition of antimony selenosulfide thin films enables solar cells with 10% efficiency," *Nature Energy*, vol. 5, no. 8, pp. 587–595, 2020.

[58] A. Chirilă, S. Buecheler, F. Pianezzi et al., "Highly efficient Cu(In,Ga)Se_2 solar cells grown on flexible polymer films," *Nature Materials*, vol. 10, no. 11, pp. 857–861, 2011.

[59] B. Bob, B. Lei, C.-H. Chung et al., "The development of hydrazine-processed Cu(In,Ga)$(Se, S)_2$ solar cells," *Advanced Energy Materials*, vol. 2, no. 5, pp. 504–522, 2012.

[60] S.-C. Liu, Y. Yang, X. Zhang et al., "Tuning the optical absorption property of GeSe thin films by annealing treatment," *Physica Status Solidi Rapid Research Letters*, vol. 12, no. 12, Article ID 1800370, 2018.

[61] Z. Li, X. Liang, G. Li et al., "9.2%-efficient core–shell structured antimony selenide nanorod array solar cells," *Nature Communications*, vol. 10, no. 1, pp. 1–9, 2019.

[62] R. F. Pierret, *Semiconductor Device Fundamentals*, Addison Wesley Publishing Company, 2nd edition, 1996.

[63] M. Wautelet, "On the physics of micromachines," *European Journal of Physics*, vol. 20, no. 3, pp. L29–L30, 1999.

[64] K. C. Kao, "Charge carrier injection from electrical contacts," in *Dielectric Phenomena in Solids*, K. C. Kao, Ed., pp. 327–380, Academic Press, San Diego, 2004.

[65] B. E. Filali, O. Y. Titov, and Y. G. Gurevich, "Physics of charge transport in metal-monopolar (*n*- or *p*-type) semiconductor-metal structures," *Journal of Physics and Chemistry of Solids*, vol. 118, pp. 14–20, 2018.

[66] P. Sawicka-Chudy, M. Sibiński, G. Wisz, E. Rybak-Wilusz, and M. Cholewa, "Numerical analysis and optimization of Cu_2O/TiO_2, CuO/TiO_2, heterojunction solar cells using SCAPS," *Journal of Physics: Conference Series*, vol. 1033, Article ID 12002, 2018.

[67] W. Zi, F. Mu, X. Lu et al., "Post-annealing treatment of a-GeSe thin films for photovoltaic application," *Solar Energy*, vol. 199, pp. 837–843, 2020.

[68] J. Hossain, B. K. Mondal, and S. K. Mostaque, "Computational investigation on the photovoltaic performance of an efficient GeSe-based dual-heterojunction thin film solar cell," *Semiconductor Science and Technology*, vol. 37, no. 1, Article ID 15008, 2021.

[69] X. Zhao, Y. Liang, L. Xue, G. Li, and F. Guo, "Numerical simulation and performance optimization of GeSe based thin film solar cell with NiO as back surface field layer," *Optical Materials*, vol. 131, Article ID 112707, 2022.

[70] J.-M. Wu, Y.-P. Lv, H. Wu et al., "Stable GeSe thin-film solar cells employing nontoxic SnO_2 as buffer layer," *Rare Metals*, vol. 41, no. 9, pp. 2992–2997, 2022.

[71] R. Roesch, T. Faber, E. Von Hauff, T. M. Brown, M. Lira-Cantu, and H. Hoppe, "Procedures and practices for evaluating thin-film solar cell stability," *Advanced Energy Materials*, vol. 5, no. 20, Article ID 1501407, 2015.